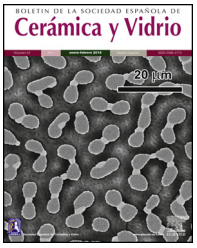
BOLETIN DE LA SOCIEDAD ESPAÑOLA DE
Cerámica y Vidrio
www.elsevier.es/bsecv



Evaluation of the impact of Izmit Gulf bottom mud on the microstructure and technical properties of porcelain tiles

Nermin Demirkol[a,*], *Neslihan Tamsü Selli*[b]

[a] *Department of Ceramics, Kocaeli University, Cedit Street, İzmit 41100, Kocaeli, Turkey*
[b] *Department of Material Science and Engineering, Gebze Technical University, Cumhuriyet Street, Gebze 41400, Kocaeli, Turkey*

ARTICLE INFO

Article history:
Received 10 June 2025
Accepted 28 July 2025
Available online 23 August 2025

Keywords:
Izmit Gulf
Bottom mud waste
Microstructure
Porcelain tile
Sustainability

ABSTRACT

Recycling waste, using new potential local raw materials, and ecological practices have become necessary in today's world. This study added Izmit Gulf bottom mud waste as a replacement for clay in porcelain tile compositions at 5%, 10%, and 15% by weight (both in its natural form and its form calcined at 1000 °C). The samples sintered under industrial heating at 1220 °C were evaluated for firing shrinkage, density, green and fired flexural strength, and water absorption values and compared with standard porcelain tiles. Phase analysis was carried out using X-ray diffraction, and microstructural characteristics were examined using a scanning electron microscope. Notably, the samples containing 10% bottom mud showed green strength twice as high as the standard and a maximum fired strength of 85 MPa. X-ray diffraction revealed the formation of quartz, mullite, and sillimanite crystals in the waste-added samples. Calcination reduced the fluxing components and adversely affected rheology, making the natural form of waste more effective. At 15% addition, porosity increased, leading to deterioration in mechanical and physical properties. The A3 composition studied here is proposed as a promising alternative for producing a more sustainable, affordable, and environmentally friendly porcelain tile product.

© 2025 The Authors. Published by Elsevier España, S.L.U. on behalf of SECV. This is an open access article under the CC BY-NC-ND license (http://creativecommons.org/licenses/by-nc-nd/4.0/).

Evaluación del impacto del lodo del fondo del golfo de Izmit en la microestructura y las propiedades técnicas de los azulejos de porcelana

Palabras clave:
Golfo de Izmit
Residuos de lodos de fondo
Microestructura
Gres porcelánico
Sostenibilidad

RESUMEN

El reciclaje de residuos, el uso de nuevas materias primas locales y las prácticas ecológicas son hoy esenciales. En este estudio, se añadieron lodos del fondo del golfo de Izmit como sustitutos de la arcilla en composiciones de baldosas de porcelana al 5, 10 y 15% en peso, en forma natural y calcinada (1000 °C). Las muestras fueron sinterizadas a 1220 °C

* *Corresponding author.*
E-mail address: nermin.demirkol@kocaeli.edu.tr (N. Demirkol).
https://doi.org/10.1016/j.bsecv.2025.100458
0366-3175/© 2025 The Authors. Published by Elsevier España, S.L.U. on behalf of SECV. This is an open access article under the CC BY-NC-ND license (http://creativecommons.org/licenses/by-nc-nd/4.0/).

y evaluadas según contracción por cocción, densidad, resistencia a la flexión (en verde y cocidas) y absorción de agua, comparándolas con baldosas estándar. Se realizaron análisis de fases por difracción de rayos X y caracterización microestructural por microscopía electrónica de barrido. Las muestras con el 10% de lodo mostraron una resistencia en verde doble respecto al estándar, y una resistencia cocida máxima de 85 MPa. Se identificaron cristales de cuarzo, mullita y sillimanita. La calcinación redujo componentes fundentes y afectó negativamente la reología, favoreciendo el uso de residuos en forma natural. Con un 15% de adición, aumentó la porosidad, deteriorando las propiedades. La composición A3 se presenta como una alternativa prometedora para la fabricación de gres porcelánico más sostenible, económica y respetuosa con el medio ambiente.

© 2025 Los Autores. Publicado por Elsevier España, S.L.U. en nombre de SECV. Este es un artículo Open Access bajo la CC BY-NC-ND licencia (http://creativecommons.org/licencias/by-nc-nd/4.0/).

Introduction

Advancements in porcelain tiles stand out among the variety of products the ceramic industry offers. Porcelain tiles emerged in Italy in the late 1970s as a technically superior tile with a natural appearance, resembling natural stone or rock more closely than other ceramic products [1–4]. Porcelain tile is a fully vitrified and highly dense product with very low porosity (≤0.05% by weight). The continuous increase in global porcelain tile production capacity and growing competition encourage manufacturers and researchers to improve production technologies, reduce costs, and enhance existing materials with new functional properties [5–8]. Numerous studies in literature have investigated the utilization of process waste or natural waste in ceramic tiles [9–12]. Pinheiro and Holanda studied the reuse of solid petroleum and its derivative waste in porcelain tile production [13]. They replaced kaolin with up to 5.0% by weight of this waste material in their compositions. Guzmán et al. incorporated rice husk ash into porcelain tile compositions [14]. They prepared a standard industrial porcelain tile composition and two different compositions containing rice husk ash (used in place of feldspar). Ke et al. investigated the reuse of polishing stone waste generated during polishing processes in porcelain tiles [15]. Soares Filho et al. examined the use of brick and roof tile waste in polished porcelain tile formulations [16]. They reported that compositions containing 15.0% by weight of brick and roof tile waste exhibited approximately a 14-unit increase in brightness compared to waste-free compositions. Bahtlı and Erdem studied the use of waste casting sands as a replacement for clay and kaolin in porcelain tile production [17]. Ozturk et al. researched the use and recycling of filter process bottom mud waste in porcelain tile formulations [18]. Global issues such as the raw material crisis during the pandemic have recently increased the focus on lower-cost and locally available alternative raw materials in ceramic tile production. Evaluating alternative raw materials, such as industrial by-products and natural environmental waste, in porcelain tile compositions remains a prominent research topic.

The aim of this study is to develop new tile compositions by incorporating bottom mud from İzmit Gulf into porcelain mixtures at specific ratios. The study discusses the microstructural, physical, and mechanical properties created in porcelain tiles by both the natural form of the waste and its form after being calcined at 1000 °C to eliminate impurities and organic compounds.

Table 1 – Chemical analysis of İzmit Gulf bottom mud.

Components	Sediment	Sediment (after 1000 °C calcination)
	(wt. %)	(wt. %)
Al_2O_3	15.74	15.71
SiO_2	44.64	57.68
Na_2O	3.86	1.81
CaO	6.56	6.39
TiO_2	0.87	0.81
MgO	3.07	2.83
K_2O	2.36	0.29
Fe_2O_3	7.47	4.66
P_2O_5	0.15	0.21
MnO	0.07	0.06
L.O.I	15.21	9.55

Experimental procedure

İzmit Gulf bottom mud analyses and sample preparation

Chemical analysis of the segment was carried out using XRF analytical equipment (Epson 4 X-Ray Spectrometer, Malvern Panalytical), and the results are shown in Table 1. As a result of the chemical analysis, the waste was found to contain high amounts of silica, alumina, iron oxide, calcium oxide, magnesium oxide, sodium oxide, and potassium oxide, respectively. Following this, after calcination at 1000 °C, an increase in the amount of SiO_2 in the waste material was observed, while a decrease in the amounts of Na_2O, K_2O, MgO, and Fe_2O_3 were noted. The L.O.I value of the raw sediment was found to be 15.21%, whereas it decreased to 9.55% after calcination at 1000 °C. This reduction indicates the elimination of volatile components such as bound water, organic matter, and possibly carbonates or hydroxyl-containing phases. The significant mass loss suggests that the sediment contains a considerable amount of thermally unstable constituents, which may influence densification and phase evolution during firing.

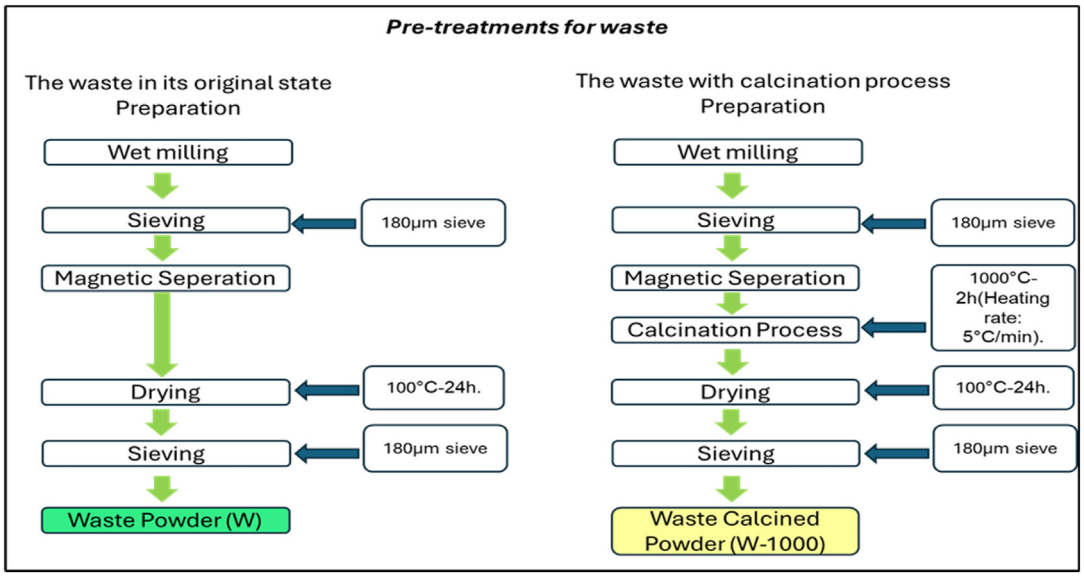


Fig. 1 – Flow chart showing the pre-treatment processes of the wastes.

Table 2 – Composition details.

Component (wt.%)	Composition codes						
	STD	A1	A2	A3	A4	A5	A6
Clay	45.0	40.0	40.0	35.0	35.0	30.0	30.0
Kaolin	10.0	10.0	10.0	10.0	10.0	10.0	10.0
Sodium feldspar	25.0	25.0	25.0	25.0	25.0	25.0	25.0
Potassium feldspar	20.0	20.0	20.0	20.0	20.0	20.0	20.0
Waste (W)	–	5.0	–	10.0	–	15.0	–
Waste (W_1000)	–	–	5.0		10.0	–	15.0

The next step involved evaluating the preparation process of dredged sediment waste and the preparation process of the waste obtained after calcination, which are given in Fig. 1. Particle size analysis of the powders from pre-treated waste was performed using the laser diffraction method (Malvern Master Sizer 2000). Based on these characterizations, the porcelain tile preparation process was initiated. Since the chemical analysis of the waste compositions indicated they could be used as a substitute for clay composition, they were partially incorporated in place of clay at weight ratios of 5%, 10%, and 15%. The components, in the proportions specified in Table 2, were weighed to formulate the recipes.

To ensure uniformity, the recipes were prepared based on 200 g of total material. A solid content of 60% was maintained, and 0.2 g of sodium silicate was added. The formulations were ground in a ball mill for 40 min. The resulting slurries were sieved through a 180 µm mesh. The sieved slurries were dried at 100 °C for 24 h in a furnace. After drying, the slurries were moistened to 5% and then pressed into 50 mm diameter tablets using a Gabrielli laboratory press at a pressure of 44 bar. The standard composition was sintered in a Nannetti laboratory-type fast-firing furnace at 1220 °C for 37 min.

Finally, after sintering, the water absorption value of the samples was determined by water saturation under vacuum and Archimedes' principle (ISO 10545-3) [19,20]. Firing shrinkage value of the samples was calculated [21].

Determination of the effects of wastes on the viscosity of porcelain tile slurry

During the preparation of porcelain tile compositions, viscosity measurements were conducted to determine whether the wastes affected the viscosity of the porcelain tile slurry. An Anton Paar (ViscoQC-100R) viscometer was used for this purpose. The temperature was maintained at 25 °C, and the sample was mechanically pre-mixed at 850 RPM for 1 min, followed by a resting period of 1 min before the test commenced. To observe the settling behavior of the bottom slurry waste, time-dependent viscosity values were also examined. Viscosity values at 1, 5, 10, 30, 60, and 120 min were measured, and the results were compared with those of a standard porcelain tile sample.

Measurement of the flexural strength values of the samples

The waste-added samples were shaped into pellets and also pressed into dimensions of 7 mm × 75 mm × 39 mm (Instron Ltd., Model 5569). The green and fired strength values of these samples were measured using a strength testing device. The measurements for each sample have been repeated 5 times.

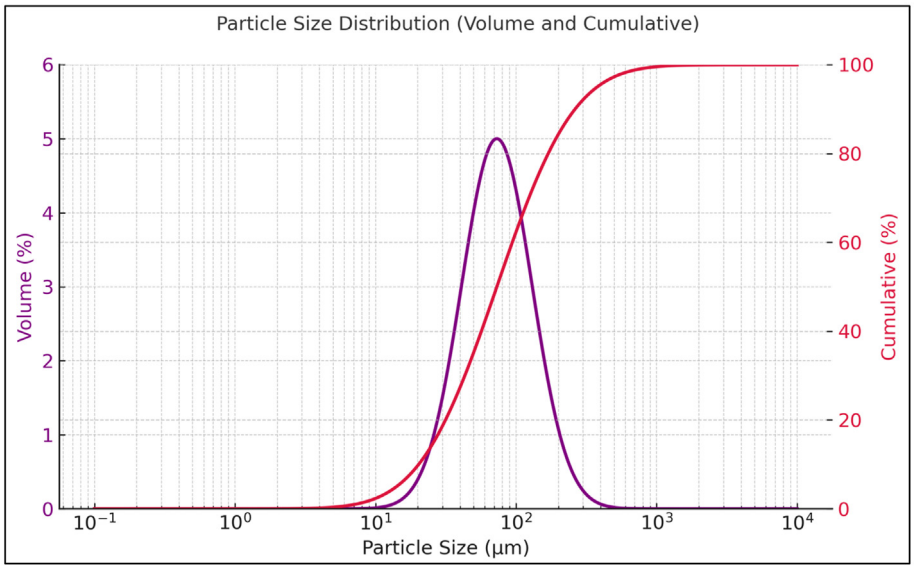


Fig. 2 – The graph of particle size analysis of waste.

XRD and SEM/EDX analysis of the samples

As XRD analyses were conducted on the waste samples before and after calcination, XRD analyses were also performed on the fired samples containing waste. For XRD analysis, Panalytical Empyrean diffractometer working at 40 kV and 40 mA was used. They were scanned at 2°/min speed in the range of 5–70° with CuKα radiation (λ = 0.154 nm). Scanning electron microscopy (SEM) and energy-dispersive X-ray spectroscopy (EDX) analysis were performed to examine the microstructure and phases formed in the samples after sintering. The analysis was conducted by a Phillips XL30 SFEG scanning electron microscope. SEM specimens' surface was ground and polished, then chemically etched in HF solution to remove the glassy phase and reveal the crystalline phases and coated with gold/carbon.

Results and discussion

Particle size distribution and mineralogical analysis of waste

In Fig. 2, the particle size analysis result of the waste was presented. Overall, examining the results indicates that the particle size distribution changes in a unimodal structure. According to this graph, the waste material shows that 10% of the particles are smaller than 6.57 μm. The average particle size consists of particles smaller than 72.79 μm. It can be observed that 90% of the particles are smaller than 264.40 μm. No issues were encountered during the grinding of the waste, and the grinding process was carried out easily.

In Fig. 3, shows the XRD patterns of the raw sediment sample (W) and the same sample after calcination at 1000 °C (W – 1000). The raw sediment is characterized by distinct peaks of calcite ($CaCO_3$) and minor peaks of quartz. After calcination at 1000 °C, calcite peaks disappear, indicating thermal decomposition of carbonate phases, which is also consistent

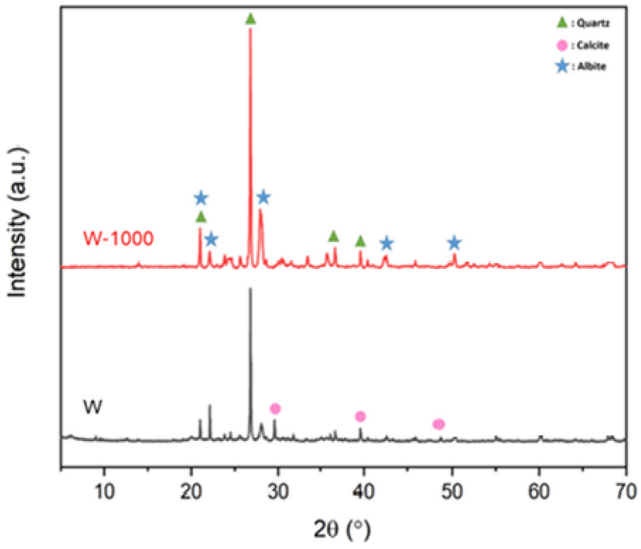


Fig. 3 – XRD patterns of the samples before calcination (W) and after calcination (W – 1000).

with the observed mass loss (L.O.I decrease from 15.21% to 9.55%). In contrast, the W – 1000 sample exhibits dominant peaks of quartz and newly developed peaks attributed to albite ($NaAlSi_3O_8$), suggesting a phase transformation or crystallization promoted by heat treatment. The relative increase in SiO_2 content from 44.64% to 57.68% also supports this crystallization behavior.

Effects of waste materials on the porcelain tile slip rheology

The bar chart presented in Fig. 4 illustrates the viscosity (mPa s) variation over time (seconds) for seven different series of porcelain tile slurries with varying amounts and types of waste materials. The viscosity of all series increases over time.

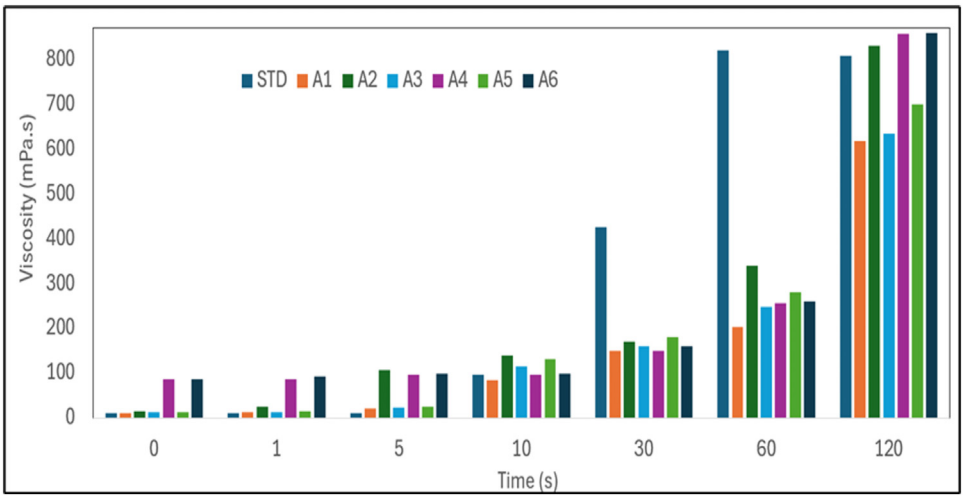


Fig. 4 – The graph showing the change in the viscosity of samples over time.

Initially (0-10 s), the viscosity values are relatively low. However, a significant increase is observed after 30 s. At 120 s, all series reach their maximum viscosity values. STD shows the highest viscosity increase over time, followed closely by A6 (%15 calcined waste bottom mud). A1 (%5 waste bottom mud) and A3 (%10 waste bottom mud) display a more gradual increase in viscosity. A2 (%5 calcined waste bottom mud) and A4 (%10 calcined waste bottom mud) have slightly higher viscosity values than their non-calcined counterparts. A5 (%15 waste bottom mud) has a lower viscosity at 120 s compared to A6 (%15 calcined waste bottom mud), indicating that calcination has an impact on increasing viscosity.

The results indicate that higher bottom mud content leads to increased viscosity due to the presence of additional solid phases and their water absorption effects. As the bottom mud content rises, the number of solid particles in the slurry increases, restricting fluidity and leading to a more viscous system. This phenomenon is particularly evident at higher bottom mud concentrations, where the dispersion medium struggles to maintain a stable suspension. Furthermore, calcined bottom mud exhibits a more pronounced impact on viscosity compared to raw bottom mud. This can be attributed to its modified structure and potentially higher surface activity after thermal treatment. The calcination process alters the microstructure of the bottom mud, enhancing its ability to interact with the dispersion medium and increasing the tendency for particle agglomeration.

Evaluation of mechanical and technological properties of the samples

The green strength results of the standard and waste-added samples are given in Fig. 5. The standard sample (STD) exhibited the lowest strength, suggesting limited mechanical stability in the green state. Among the modified samples, A3 demonstrated the highest green flexural strength, exceeding 1.2 MPa, indicating a substantial improvement in mechanical integrity before sintering. Samples A1, A2, A4, and A5 showed moderate enhancements, while A6 displayed a lower strength, similar to the standard sample. The variation in green flexural strength can generally be attributed to differences in particle packing, bonding characteristics, and the water retention capacity of the composition components [22–24]. Notably, adding waste in its non-calcined form improved cohesion by increasing the overall plasticity of the composition, leading to better compaction and higher green strength. However, the calcination of the waste and its addition in higher amounts disrupted particle bonding, reduced plasticity, and resulted in the formation of weaker structures.

The flexural strength of the fired samples (Fig. 6) exhibits significant variations based on the type and amount of bottom mud added to the porcelain composition. The standard porcelain (STD) shows the lowest flexural strength among all samples. However, adding 5% and 10% non-calcined mud (A1 and A3) substantially increases flexural strength, with A3 achieving the highest value. This suggests that the fluxing effect of the mud components enhances sintering and densification, opening promising avenues for the use of non-calcined mud in improving the mechanical properties of porcelain. However, the flexural strength declines as the bottom mud content increases beyond 10% (A5 and A6). The calcined bottom mud samples (A2, A4, and A6) generally exhibit lower strength than their non-calcined counterparts. This suggests that calcination is crucial in altering material properties and reducing densification and bonding efficiency. Therefore, while moderate additions of non-calcined dredge bottom mud can improve mechanical performance, excessive amounts or the use of calcined bottom mud can negatively impact the structural integrity of the final product.

Table 3 presents the technological properties of porcelain tile samples, including firing shrinkage, water absorption, and bulk density. The results indicate that samples A5 and A6 exhibit significantly lower bulk densities (1.90 g/cm^3 and 1.70 g/cm^3, respectively) than the standard composition (2.25 g/cm^3). This decrease in density can be attributed to the higher waste content (15%) in these compositions, which likely led to increased porosity formation during firing. Additionally, calcination appears to impact bulk density across

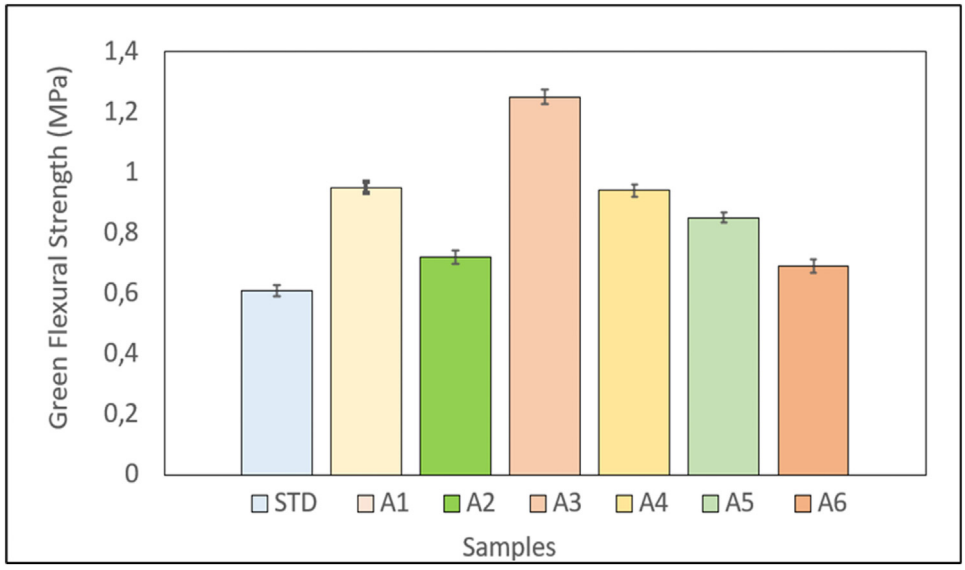


Fig. 5 – Graph showing the green strength results of the samples.

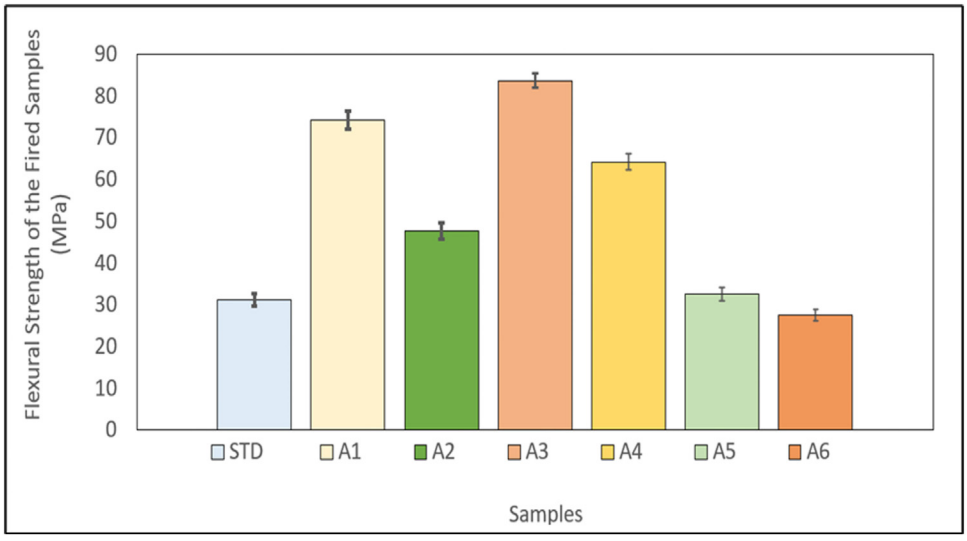


Fig. 6 – Flexural strength values of the samples after firing.

Table 3 – Technological properties of the porcelain tiles.

Samples	Firing shrinkage (%)	Water absorption (%)	Bulk density (g/cm^3)
STD	7.5 ± 0.2	0.52 ± 0.01	2.25 ± 0.3
A1	9.2 ± 0.1	0.33 ± 0.01	2.46 ± 0.2
A2	8.2 ± 0.2	0.46 ± 0.01	2.33 ± 0.1
A3	10.1 ± 0.1	0.01 ± 0.01	2.64 ± 0.2
A4	8.6 ± 0.2	0.15 ± 0.01	2.39 ± 0.2
A5	6.19 ± 0.2	1.68 ± 0.01	1.90 ± 0.2
A6	6.02 ± 0.1	2.05 ± 0.01	1.70 ± 0.2

all samples negatively. This effect can be explained by the thermal decomposition and phase transformations occurring during the pre-calcination process, which may cause structural changes in the waste material, increasing its porosity. As a result, the incorporation of calcined waste (A2, A4, A6) tends to yield lower densities than their raw waste counterparts (A1, A3, A5). Furthermore, the significant increase in water absorption in A5 (1.68%) and A6 (2.05%) suggests that the porosity within these samples is more interconnected, further reducing their bulk density and mechanical integrity.

The chemical composition of the bottom mud includes significant amounts of Na_2O, K_2O (alkalies), CaO (alkaline earth), and Fe_2O_3. These oxides act as fluxing agents that lower the liquidus temperature and promote early formation of a liquid phase during firing [25–28]. These alkali oxides strongly enhance liquid phase formation, with initial melt-

ing points in the SiO_2–Al_2O_3–alkali systems starting around 980–1050 °C [25]. Their presence accelerates sintering and densification, which explains the improved mechanical properties at 5–10% mud addition. CaO contributes to the formation of a more viscous liquid phase and reacts with silica and alumina to lower the melting temperature [26]. Fe_2O_3 further affects viscosity and promotes the stabilization of iron-bearing crystalline phases, such as Fe-substituted sillimanite. According to phase diagrams, the initial liquid phase formation in the SiO_2–Al_2O_3–CaO and SiO_2–Al_2O_3–Fe_2O_3 systems begins around 1100–1150 °C [25–27]. These fluxing effects justify the densification and strength increase observed in compositions A1 and A3. However, excessive fluxing (15% mud) led to higher porosity and lower bulk density due to over abundant liquid phase and pore coalescence during firing.

Phases and microstructural properties of the samples

The XRD analysis of the fired samples reveals significant phase transformations influenced by adding bottom mud in the samples, as shown in Fig. 7(a). Quartz (PDF #01-083-0539) has been identified as the dominant phase in the standard porcelain tile body (STD). However, with the addition of dredge bottom mud, a noticeable decrease in quartz peaks is observed, particularly in samples containing 15% bottom mud (A5 and A6). This indicates that phase transformations accelerate as the bottom mud content increases, and the reactive oxides in the bottom mud composition interact with the ceramic matrix. Mullite (PDF #15-0776) is a crucial phase that enhances porcelain ceramics' strength [29,30] and thermal resistance [31–35]. Additionally, peaks corresponding to the sillimanite phase are observed in all samples. Sillimanite (PDF #00-041-1487) is a phase that can transform into mullite at high temperatures [36] and enhance the refractory properties of ceramic materials [37–39]. According to high-resolution synchrotron diffraction studies in the literature [36], sillimanite (Al_2SiO_5) gradually transforms into mullite ($3Al_2O_3$ $2SiO_2$) in the temperature range of approximately 1200–1250 °C. Since the samples in this study were sintered at 1220 °C, which is within this transformation interval, the simultaneous presence of sillimanite and mullite detected by XRD is scientifically justified the incomplete transformation can be attributed to kinetic limitations and the relatively short firing time. In Fig. 7(b), a magnified view of the XRD patterns of the standard (STD) and the A6 sample containing the highest amount of waste is provided to clarify the phase identification. Despite the close crystallographic parameters of mullite and sillimanite, the presence of distinct peak positions allows their differentiation. In particular, sillimanite peaks at ~26.3°, ~30.6°, and ~35.5° are visible alongside the characteristic mullite reflections (e.g., ~26.0°, ~33.1°), indicating the coexistence of both phases. The enhanced peak intensity in A6 compared to STD supports the formation of sillimanite due to the waste addition, while mullite remains as a major phase. This magnified region confirms that the assignment of overlapping peaks considers phase-specific diffraction characteristics despite limited XRD resolution.

In addition, the formation of sillimanite within the porcelain matrix due to the addition of dredge bottom mud may positively influence the ceramic's high-temperature resistance. When the results are evaluated, it is evident that adding dredge bottom mud reduces quartz content while increasing mullite and sillimanite formation. This beneficial effect potentially improves porcelain ceramics' mechanical and thermal properties [40,41]. In this study, high mechanical strength obtained after firing also supports this finding (Fig. 6).

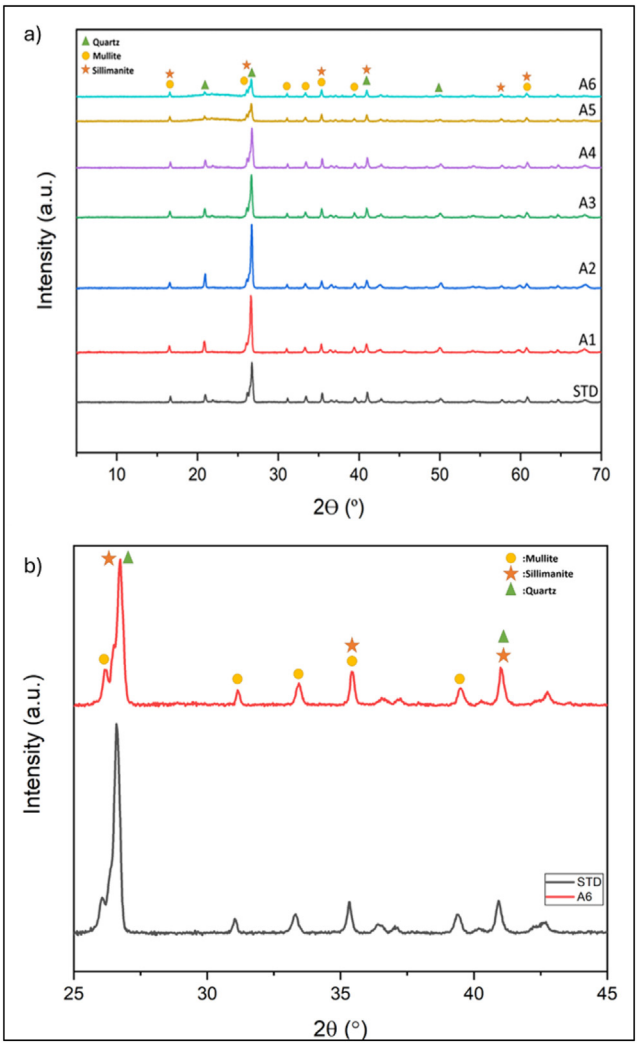


Fig. 7 – XRD analysis results of the samples after firing. (a) All samples. (b) Enlarged view of the peaks for STD and A6 samples.

Fig. 8 presents the microstructures of the chemically etched waste-added samples after firing. In all samples, angular large-grained crystals, rod-like crystals, and rectangular prism-shaped rod-like crystals are prominent. EDX analyses were conducted to identify the crystals. The microstructure of the standard porcelain tile sample (STD) and the chemically etched microstructure of the A3 sample are presented in Fig. 9(a) and (b), respectively. The EDX analyses of the angular crystals labeled as "1" and the rod-like crystals labeled as "2" are shown in Fig. 9(c) and (d) – similar crystals formed in both waste-added and waste-free samples. The EDX analysis of the crystals labeled as "1" shows dominant peaks of silicon (Si) and oxygen (O), indicating the presence of quartz grains [42]. The analysis of the areas labeled as "2" reveals Si, O, and

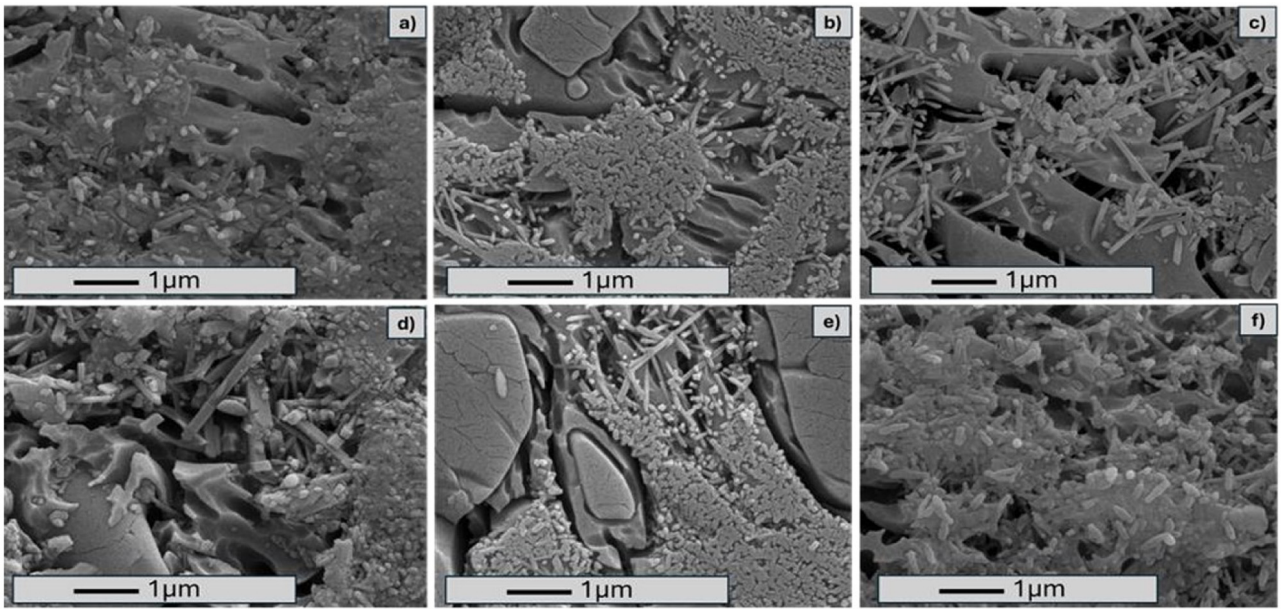


Fig. 8 – Microstructure images of the samples after firing: (a) sample A1, (b) sample A2, (c) sample A3, (d) sample A4, (e) sample A5, and (f) sample A6.

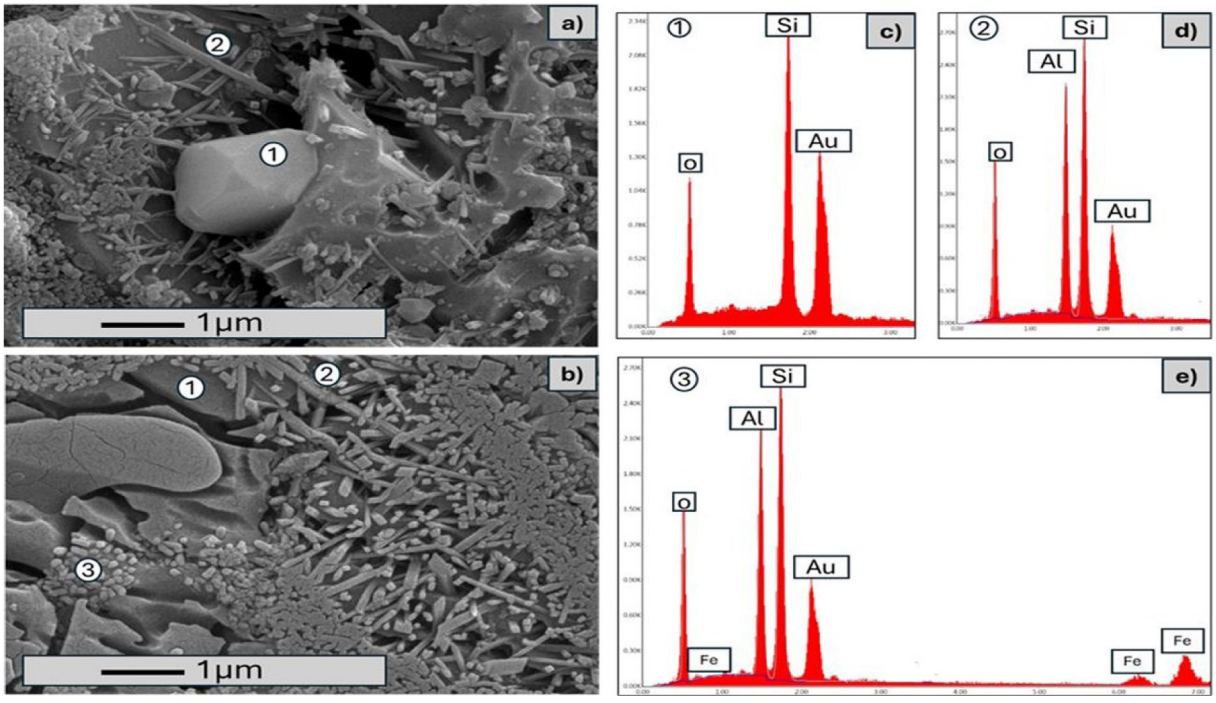


Fig. 9 – SEM images of (a) the STD sample, (b) the A3 sample, and EDX analysis of the crystals labeled as (c) 1, (d) 2, and (e) 3.

aluminum (Al) peaks, which correspond to mullite crystals [43,44]. In the A3 sample (Fig. 9(b)), which was selected as a representative example since similar phases were observed in all waste-added samples, rectangular prism-shaped rod-like crystals appear, differing from the STD sample. The EDX analysis performed on region "3" (Fig. 10(e)) shows dominant peaks of Al, Si, and iron (Fe), indicating the formation of Fe-substituted sillimanite crystals [44,45]. The gold (Au) peak observed in all samples, a result of the coating applied for microstructural analysis. All results obtained are consistent with the XRD findings (Fig. 7).

The surface microstructures of the samples after firing were also examined (Fig. 10). In the standard sample, interconnected pore structures are prominent (Fig. 10(a)). A noticeable reduction in pore size is observed in the A1 (Fig. 10(b)) and A3 (Fig. 10(d)) samples, where raw bottom mud waste was

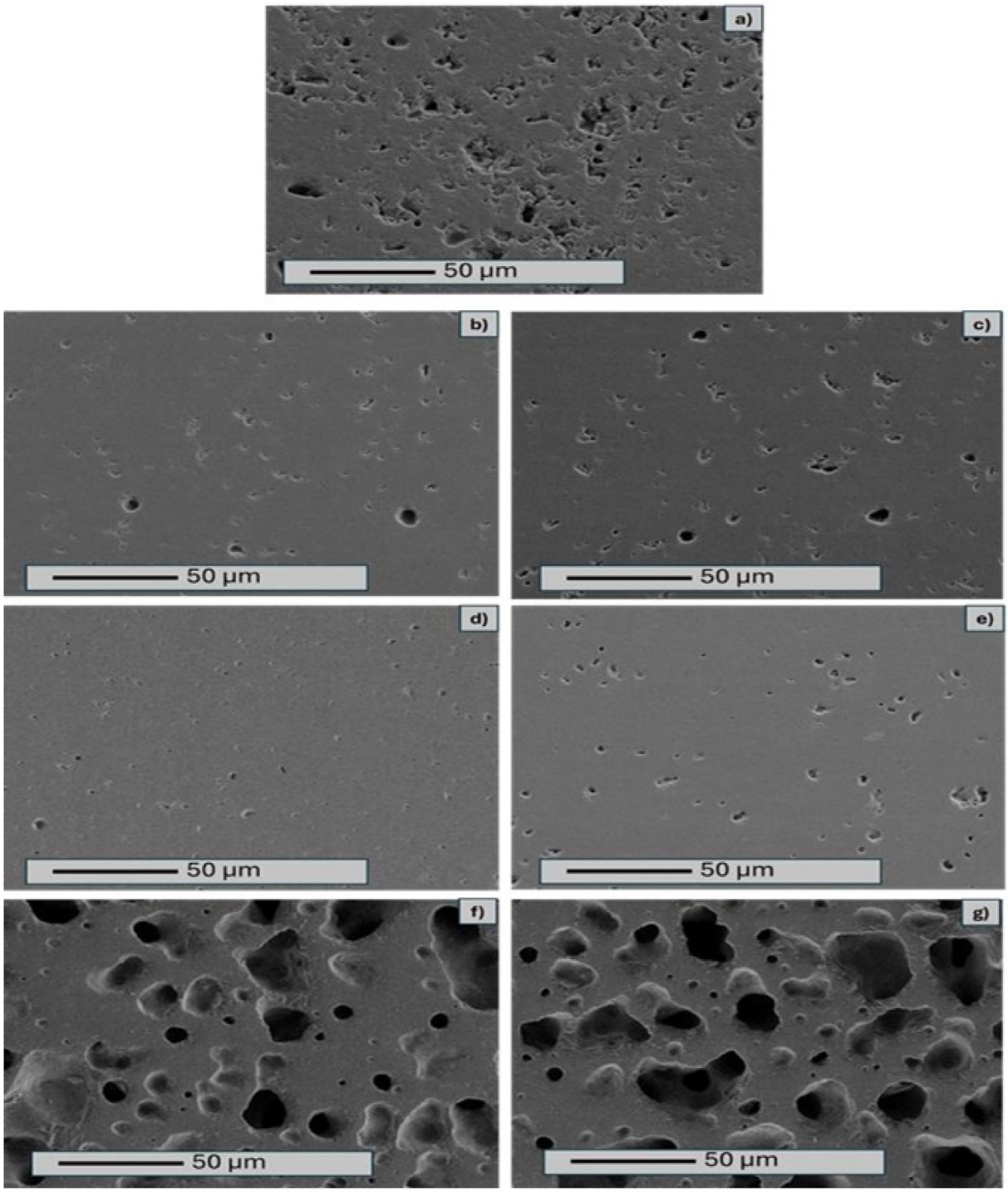


Fig. 10 – Microstructure images showing the surfaces of the samples after firing (a) STD, (b) A1, (c) A2, (d) A3, (e) A4, (f) A5) and (g) A6 samples.

used. However, the A3 sample stands out with its highly dense microstructure, a significant finding. In contrast, in the A2 (Fig. 10(c)) and A4 (Fig. 10(e)) samples, where calcined bottom mud waste was used, the pores appear to occupy a larger area and have grown compared to the A1 and A3 samples. In the A5 (Fig. 10(f)) and A6 (Fig. 10(g)) samples, where the bottom mud waste content reaches 15% by weight, coarse pores ranging in size from 10 to 35 µm are observed. The effects of these microstructural changes are also reflected in the technical properties of the porcelain tiles (Table 3).

Conclusions

This study comprehensively evaluated the effects of incorporating İzmit Gulf bottom mud into porcelain tile formulations,

and the main outcomes can be concisely summarized as follows:

- İzmit Gulf bottom mud waste was successfully incorporated into porcelain tile compositions as a partial replacement for clay. Time-dependent viscosity measurements showed that adding non-calcined waste resulted in thixotropic behavior comparable to standard porcelain slurry.
- The green strength increased with waste addition, with the A3 sample showing the highest values. Firing strength was also enhanced by adding 5–10% non-calcined waste, achieving a maximum flexural strength of approximately 85 MPa in the A3 sample.
- Adding more than 10% waste led to a decline in density and flexural strength due to increased porosity in the microstructure.
- The formation of interlocking rod-like mullite and sillimanite crystals contributed to the improved mechanical performance.
- Using bottom mud in porcelain tiles offers an environmentally sustainable approach to managing a significant waste volume in the İzmit Gulf region. Partial substitution of clay with this waste provides economic benefits by reducing raw material consumption and facilitating waste recycling.

These results demonstrate the feasibility and benefits of utilizing İzmit Gulf bottom mud as a valuable raw material in sustainable porcelain tile production.

Declaration of competing interest

The authors declare that they have no known competing financial interest or personal relationship that could have appeared to influence the work reported in this paper.

Acknowledgments

This study was carried out by Kocaeli University Participatory Research Project in collaboration with Gebze Technical University (Project No: FKA-2024-4084). Like all authors, we would like to express our gratitude to Kocaeli University Scientific Research Projects Coordination for their support.

REFERENCES

[1] E. Sánchez, Technical considerations on porcelain tile products and their manufacturing process, InterCeram: Int. Ceram. Rev. 52 (2003) 132–139.
[2] E. Sánchez, J. García-Ten, V. Sanz, A. Moreno, Porcelain tile: almost 30 years of steady scientific-technological evolution, Ceram. Int. 36 (2010) 831–845, http://dx.doi.org/10.1016/j.ceramint.2009.11.016.
[3] J.M.R.D. Figueirêdo, F.P.D. Costa, J.V. Fernandes, A.M. Rodrigues, G.D.A. Neves, R.R. Menezes, et al., Development of scheelite tailings-based ceramic formulations with the potential to manufacture porcelain tiles, semi-stoneware and stoneware, Materials 13 (2020) 5122, http://dx.doi.org/10.3390/ma13225122.
[4] A. Tucci, L. Esposito, L. Malmusi, E. Rambaldi, New body mixes for porcelain stoneware tiles with improved mechanical characteristics, J. Eur. Ceram. Soc. 27 (2–3) (2007) 1875–1881, http://dx.doi.org/10.1016/j.jeurceramsoc.2006.05.007.
[5] N. Tangboriboon, S. Pornsimma, A. Sirivat, Embedding eggshell as flux in porcelain clay products to reduce firing temperature via extrusion process, Middle East J. Sci. Res. 24 (5) (2016) 523–537.
[6] K. Dana, S. Das, K.S. Das, Effect of substitution of fly ash for quartz in triaxial Kaolin–Quartz–Feldspar system, J. Eur. Ceram. Soc. 24 (2004) 3169–3175, http://dx.doi.org/10.1016/j.jeurceramsoc.2003.10.008.
[7] M. Lassinantti Gualtieri, C. Mugoni, S. Guandalini, A. Cattini, D. Mazzini, C. Alboni, et al., Glass recycling in the production of low-temperature stoneware tiles, J. Clean. Prod. 197 (2018) 1531–1539, http://dx.doi.org/10.1016/j.jclepro.2018.06.264.
[8] M. Locks, S. Arcaro, C.P. Bergmann, M.J. Ribeiro, F. Raupp-Pereira, O.R.K. Montedo, Effect of feldspar substitution by basalt on pyroplastic behaviour of porcelain tile composition, Materials 14 (2021) 3990, http://dx.doi.org/10.3390/ma14143990.
[9] S.K. Mohammad, S. Mohammad, S.K. Noor, S. Murtaza, Industrial ceramic waste in Pakistan, valuable material for possible applications, J. Clean. Prod. 139 (2016) 1520–1528, http://dx.doi.org/10.1016/j.jclepro.2016.08.131.
[10] A. Karamanov, E. Karamanova, A.M. Ferrari, F. Ferrante, M. Pelino, The effect of fired scrap addition on the sintering behaviour of hard porcelain, Ceram. Int. 32 (2006) 727–732, http://dx.doi.org/10.1016/j.ceramint.2005.05.009.
[11] F. Altimari, F. Andreola, P.P. Benassi, I. Lancellotti, L. Barbieri, Pumice and lapillus scraps: new national environmental-friendly chance for the production of ceramic tiles, Ceram. Int. 49 (2023) 38743–38753, http://dx.doi.org/10.1016/j.ceramint.2023.09.211.
[12] E.P. Almeida, M.E.A. Carreiro, A.M. Rodrigues, H.S. Ferreira, L.N.L. Santana, R.R. Menezes, et al., A new eco-friendly mass formulation based on industrial mining residues for the manufacture of ceramic tiles, Ceram. Int. 47 (2021) 11340–11348, http://dx.doi.org/10.1016/j.ceramint.2020.12.260.
[13] B.C.A. Pinheiro, J.N.F. Holanda, Reuse of solid petroleum waste in the manufacture of porcelain stoneware tile, J. Environ. Manage. 118 (2013) 205–210.
[14] A.A. Guzmán, Á.S. Delvasto, V.M. Francisca Quereda, V.E. Sánchez, Valorization of rice straw waste: production of porcelain tiles, Cerâmica 61 (360) (2015) 442–449.
[15] S. Ke, Y. Wang, Z. Pan, C. Ning, S. Zheng, Recycling of polished tile waste as a main raw material in porcelain tiles, J. Clean. Prod. 115 (2016) 238–244.
[16] J.E. Soares Filho, J.C. Aurich, F.J.P. Sousa, R.M. Nascimento, C.A. Paskocimas, A.H.A. Silva, Polishing performance of eco-friendly porcelain stoneware tiles reusing bricks and roof tiles wastes, J. Clean. Prod. 256 (2020), 120362.
[17] T. Bahtlı, Y. Erdem, The use of foundry waste sand from investment casting in the production of porcelain tiles, Ceram. Int. 48 (19 (Part A)) (2022) 27967–27972.
[18] Z.B. Ozturk, Y. Karaca, B. Kayali, E. Ubay, The use and recycling of filter press cake wastes in eco friendly porcelain tile formulations, Int. J. Environ. Sci. Technol. 20 (2023) 6307–6318.
[19] M. Dondi, G. Guarini, C. Melandri, M. Raimondo, C. Zanelli, Resistance to impact of porcelain stoneware tiles, Ceram. Int. 42 (2016) (2016) 5731–5736, http://dx.doi.org/10.1016/j.ceramint.2015.12.104.
[20] EN ISO 10545-3, Ceramic Tiles – Part 3: Determination of Water Absorption, Apparent Porosity, Apparent Relative

Density and Bulk Density, International Standard Organization, 2018.
[21] I.S. Vilarinho, E. Filippi, M.P. Seabra, Development of eco-ceramic wall tiles with bio-$CaCO_3$ from eggshells waste, Open Ceram. 9 (2022) 100220, http://dx.doi.org/10.1016/j.oceram.2022.100220.
[22] A. Kumar, K. Mohanta, D. Kumar, O. Parkash, Green properties of dry-pressed alumina compacts fabricated using sucrose as binder, Ceram. Int. 40 (2014) 6271–6277, http://dx.doi.org/10.1016/j.ceramint.2013.11.085.
[23] A. Laursen, L.N.L. Santana, R.R. Menezes, Characterization of Brazilian Northeastern plastic clays, Cerâmica 65 (2019) 578–584, http://dx.doi.org/10.1590/0366-69132019653762579.
[24] J.L. Amorós, C. Feliu, F. Ginés, A. Agra, Mechanical strength and microstructure of green ceramic bodies, in: Qualicer, Castellón, Spain, 1996, pp. 149–168.
[25] W.D. Kingery, H.K. Bowen, Introduction to Ceramics, 2nd edition, 1976, ISBN: 978-0-671-47860-7.
[26] C. Bergoron, S. Risbud, Introduction to Phase Equilibria in Ceramics, 1984, ISBN: 0916094-58-8.
[27] E. Tiffo, A. Elimbi, J. Dika Manga, A.B. Tchamba, Red ceramics produced from mixtures of kaolinite clay and waste glass, Braz. J. Sci. Technol. 2 (2015) 1–13.
[28] D.N.P. Djonga, C. Tsamo, H. Nassai, Influence of CRT glass quantity on the properties of red mud-CRT glass ceramics fired at different temperatures, J. Mater. Sci. Eng. B 9 (7–8) (2019) 133–143.
[29] S.A. Uhland, R.K. Holman, S. Morissette, M.J. Cima, E.M. Sachs, Strength of green ceramics with low binder content, J. Am. Ceram. Soc. 84 (12) (2001) 2809–2818, http://dx.doi.org/10.1111/j.1151-2916.2001.tb01098.x.
[30] J. Anggono, Mullite ceramics: its properties structure, and synthesis, Jurnal Teknik Mesin 7 (1) (2005) 1–10.
[31] N. Montoya, F.J. Serrano, M.M. Reventós, J.M. Amigo, J. Alarcón, Effect of TiO_2 on the mullite formation and mechanical properties of alumina porcelain, J. Eur. Ceram. Soc. 30 (2010) 839–846, http://dx.doi.org/10.1016/j.jeurceramsoc.2009.10.009.
[32] B. Zhang, Y. Zheng, J. Zhao, Y. Wang, M. Li, Effect of mullite whiskers on the microstructure and mechanical properties of oil well cement, Colloids Surf. A: Physicochem. Eng. Asp. 711 (2025) 136332, http://dx.doi.org/10.1016/j.colsurfa.2025.136332.
[33] W.E. Lee, Y. Iqbal, Influence of mixing on mullite formation in porcelain, J. Eur. Ceram. Soc. 14 (2001) 2583–2586, http://dx.doi.org/10.1016/S0955-2219(01)00274-6.
[34] W.E. Lee, G.P. Souza, C.J. McConville, T. Tarvornpanich, Y. Iqbal, Mullite formation in clays and clay-derived vitreous ceramics, J. Eur. Ceram. Soc. 2 (2008) 465–471, http://dx.doi.org/10.1016/j.jeurceramsoc.2007.03.009.
[35] G. Stathis, A. Ekonomakou, C.J. Stournaras, C. Ftikos, Effect of firing conditions, filler grain size and quartz content on bending strength and physical properties of sanitaryware porcelain, J. Eur. Ceram. Soc. 24 (2004) 2357–2366, http://dx.doi.org/10.1016/j.jeurceramsoc.2003.07.003.
[36] Y. Igami, S. Ohi, A. Miyake, Silimanite–mullite transformation observed in synchrotron X-Ray diffraction experiments, J. Am. Ceram. Soc. 100 (2017) 4928–4937.
[37] S. Maity, B.K. Sarkar, Development of high-strength whiteware bodies, J. Eur. Ceram. Soc. 16 (1996) 1083–1088, http://dx.doi.org/10.1016/0955-2219(96)00033-7.
[38] S. Maity, T.K. Mukhopadhyay, B.K. Sarkar, Strength of sillimanite sand reinforced porcelain subjected to thermal shock, J. Eur. Ceram. Soc. 17 (1997) 749–752, http://dx.doi.org/10.1016/S0955-2219(96)00119-7.
[39] S. Rahman, U. Feustel, S. Freimann, Structure description of the thermic phase transformation sillimanite–mullite, J. Eur. Ceram. Soc. 21 (2001) 2471–2478, http://dx.doi.org/10.1016/S0955-2219(01)00386-7.
[40] S. Yugeswaran, M. Vijay, K. Suresh, P.V. Ananthapadmanabhan, Z. Karoly, J. Szépvölgyi, Synthesis of mullite from sillimanite dissociation through transferred arc plasma torch, Int. J. Miner. Process. 99 (2011) 54–60, http://dx.doi.org/10.1016/j.minpro.2011.04.002.
[41] M.H. Hussin, N.A. Che Lah, Microstructural characterization of silica-based granite stones using field emission SEM–EDXS, Mater. Today Proc. 75 (2023) 84–90, http://dx.doi.org/10.1016/j.matpr.2022.10.105.
[42] W. Wang, Z. Shi, Z. Wang, S. Wang, Phase transformation and properties of high-quality mullite ceramics synthesized using desert drift sands as raw materials, Mater. Lett. 221 (2018) 271–274, http://dx.doi.org/10.1016/j.matlet.2018.03.162.
[43] E.A. Rodríguez, L. Díaz-Tato, J.F. López-Perales, Y. González-Carranza, Effect of binary raw materials replacement (quartz and feldspar) for porcelain chamotte on the electro-technical siliceous porcelain properties, Front. Mater. 10 (2023) 1–15, http://dx.doi.org/10.3389/fmats.2023.1322898.
[44] D.L. Whitney, Coexisting andalusite, kyanite, and sillimanite: sequential formation of three Al_2SiO_5 polymorphs during progressive metamorphism near the triple point, Sivrihisar, Turkey, Am. Mineral. 87 (2002) 405–416, http://dx.doi.org/10.2138/am-2002-0404.
[45] M. Ju, D. Gao, P. Cong, X. Zhang, W. Cai, Study on mullitization of sillimanite group minerals and its effect on properties of the Al_2O_3–SiC–C gunning material, Int. J. Appl. Ceram. Technol. 21 (6) (2024) 3981, http://dx.doi.org/10.1111/ijac.1486.